Nanoscale

Accepted Manuscript

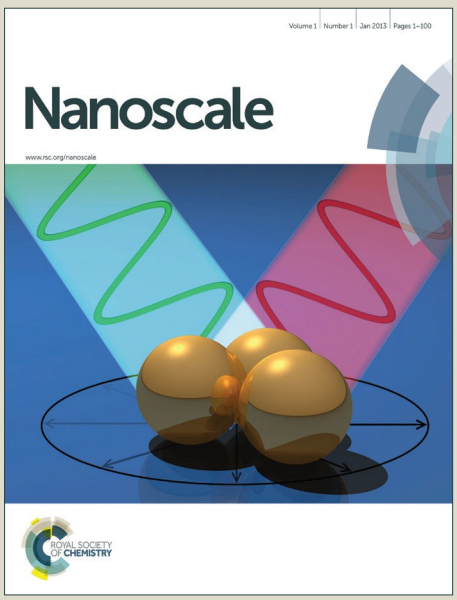

ROYAL SOCIETY OF CHEMISTRY

www.rsc.org/nanoscale

Nanoscale frictional characteristics of few layers graphene over Ni grain and interface boundaries

Manoj Tripathi[1], Firas Awaja[1], Guido Paolicelli[2], Ruben Bartali[1], Erica Iacob[1], Sergio Valeri[3], Seunghwa Ryu[4], Stefano Signetti[5], Giorgio Speranza[1], Nicola Maria Pugno* [5, 1, 6]

[1]Centre for Materials and Microsystems, Fondazione Bruno Kessler, via Sommarive 18, I-38123 Povo (Trento), Italy

[2]CNR, Istituto Nanoscienze - Centro S3, Via Campi 213/a,41125 Modena, Italy

[3]Dipartimento di Scienze Fisiche Informatiche e Matematiche, Università di Modena e Reggio Emilia,via Campi 213/a, 41125 Modena, Italy

[4]Department of Mechanical Engineering, Korea Advanced Institute of Science and Technology, Daejeon 34141, Korea

[5]Laboratory of Bio-Inspired and Graphene Nanomechanics, Department of Civil, Environmental and Mechanical Engineering, University of Trento, via Mesiano 77, I-38123 Trento, Italy

[6]School of Engineering and Materials Science, Queen Mary University of London, Mile End Road, E1 4NS London, UK

*Corresponding author: nicola.pugno@unitn.it

Abstract: The tribological properties of metal supported few layered graphene (FLG) depend strongly on the grain topology of the metal substrate. Inhomogeneous distribution of graphene layers at such regions led to variable landscapes with distinguishable roughness. This discrepancy in morphology significantly affects the wetting and frictional characteristics of the FLG system. We individually measured friction characteristics of FLG covering grains and interfacial grain boundaries of polycrystalline Ni metal substrate via an Atomic Force Microscopy (AFM) probe. The friction coefficient

of FLG covered at interfacial grain boundaries is found to be lower than that on grains in vacuum (at 10^{-5} Torr pressure) and similar results were obtained in air condition. Sliding history with AFM cantilever, static and dynamic pull-in and pull-off forces were addressed in the course of friction measurements to explain the role of the out-of-plane deformation of graphene layer/s. Finite element simulations show good agreement with experiments and led to rationalize the observations. Thus, with interfacial grain boundaries the FLG tribology can be effectively tuned.

Keywords: Atomic Force Microscopy, Finite Element Simulation, Graphene, Friction, Adhesion, Wettability

Freely suspended graphene is attractive in science due to its extraordinary properties[1, 2]. However, its interaction with a substrate, like metals plays a vital role to fill the gap between science and technological applications, like heterogeneous catalyst[3], strengthening components[4, 5], transparent electrodes[6], metallic N/MEMS[7, 8], among others. Graphene can enhance the water contact angle[9] and displays high mechanical strength, stiffness, inertness and stability[10, 11, 12] which offers durable, rust proof and antiwear coatings[13]. At micro-nano tribocontacts, where liquid state lubricant squeeze out under pressure condition[14], graphene could be used as thinnest solid state lubricant[15, 16]. Researchers have observed that graphene substantially reduces the friction force relative to the substrate on which it is coated. Filleter *et al.*[17] measured coefficient of friction (COF) of 0.004 and 0.001 for epitaxial grown monolayer and bi-layer graphene respectively over SiC (0001) in UHV condition using a polycrystalline diamond coated tip. The friction forces are nearly 25 times lower than on carbon-rich interface and nearly half than those of graphite. Marsden *et al.*[18] obtained a COF of 0.12-0.18 for CVD Gr-Cu and 0.7±0.2 for bare Cu substrate using silica tip in air condition. Using similar type of tip configuration, Egberts *et al*.[19] obtained COF almost statistically indistinguishable from zero (–0.004 ± 0.009) for Gr-Cu compared to 0.57±0.03 for the bare copper substrate in air condition. Berman *et al.*[20] observed that CVD grown few layered graphene (about 6-7 in numbers) on Ni has lower friction than silica substrate (ratio ~1/19) and Highly Ordered Pyrolytic Graphite (HOPG, ratio ~1/2). Similar investigation has been carried out by Kim *et al*[16] at both

micro and nanoscale, where they measured COF of 0.03 between fused silica lens and CVD grown Gr-Ni in air condition. They found decrease in real contact area between fused silica lens (as slider) and the graphene. The stronger adhesion between graphene and underlying Ni substrate responsible for such lowest COF than graphene on other substrates (Cu and SiO_2). Additionally, higher roughness of FLG on Ni also contributed to decrease in real contact area between fused silica lens and graphene.

Graphene produced from either mechanical exfoliation[21] or from thermal decomposition[22] shows layer and substrate dependent characteristics. Different mechanical responses have been observed for substrate supported graphene under FFM operations at nanoscale. In one case, loosely adhered graphene to substrate (like Gr-SiO_2 system) interacts strongly with sliding AFM tip due to relative higher adhesion and buckled locally followed by out-of-plane deformation. It causes an increase in contact area around the tip apex in scanning direction and resists its motion causing higher friction. This phenomenon is called "puckering"[21] that relatively enhances in case of exposed graphene (top graphite layer) in ambient air condition[23]. A theoretical follow-up attributed this behaviour to a non-destructive form of viscoelastic ploughing[24]. In another case, an increased resistance to out-of-plane deformation, and correspondingly, lower friction could be achieved through strong interaction with substrate (like mica[25], Ni[26, 27] etc.). Molecular dynamics simulations demonstrated that stacked graphene would be a better lubricant to lower down friction for an AFM tip than loosed graphene[24]. Several reports suggested functionalized graphene (e.g. adsorption with fluoride ion, hydrogen etc.) to raise out-of-plane bending stiffness. Chemically modified graphene with adsorption of third body (like hydrogen and fluoride ions) enhances friction at the nanoscale between slider and substrate[28, 29] even up-to 4-folds in case of fluorination.

There is still limited understanding of the frictional characteristics of graphene and its behaviour over different substrates, especially for metallic support. All of the results described above for metal-supported graphene did not include the influence of metal grains and grain boundaries on the frictional characteristics of graphene. Our previous investigation revealed that a single layer of graphene grown on Ni (111) crystal shows lower friction force than graphite against silica tip in vacuum[30]. Here, we are

proposing a new criteria that influence tribology of graphene at the interfacial grain boundaries of the substrate (here Ni is considered as a case study). From tribological perspective, graphene on polycrystalline Ni (Gr/Ni-P) is a composite system equivalent to graphite (HOPG, Highly Ordered Pyrolytic Graphite) but with finite layers, possess higher roughness (nearly 70 times) due to presence of interfacial grain boundaries and randomly oriented plane of Ni grains. Our current work is different from reported literature at microscale[16], where friction measurement has accumulated results from grain and interfacial grain boundaries. We differentiated friction forces from grains and interface grain boundaries and resolved their contributions exclusively. In our present work, series of investigation are as follows: in the first part, morphology of Gr/Ni-P has been discussed. In second part, morphological influence over wettability has been described. In the final section, we showed morphological influence over frictional characteristics of graphene in vacuum condition using graphene covered grain domain and interface grain boundaries.

Results and discussion

Morphological description of bare polycrystalline Ni and CVD grown graphene on polycrystalline Ni.

Polycrystalline Ni metal contains surfaces features/regions that are randomly oriented, relative to each other, and are separated by thin boundary areas. We term those regions as “Ni grain” and “Ni interface boundary” (Ni-IB) respectively, throughout the manuscript. A typical example of polycrystalline nickel metal substrate is presented in Fig. 1(a). This is a 3-D AFM image where Ni grains and Ni-IB are clearly visible. The average roughness R_a of a particular grain region (size 600 x600 nm^2) is nearly 0.2 nm while for entire image area (2x2 μm^2 that includes several interface regions) R_a increases to 0.3 nm. At fig. 1(b), the friction force measured on the same Ni region is presented. The friction signal is higher at Ni-IB than on Ni grain due to the involvement of the extra atom at the edges felt by tip apex[31]. During CVD

operations these Ni-IBs potentially are suitable nucleation sites for multilayer graphene during segregation-growth mechanism[32]. Therefore, pronounced roughness is expected for the graphene-covered polycrystalline Ni (Gr/Ni-P) with abundant Ni-IB, since it facilitates the formation of multilayer graphene at Ni-IB due to higher availability of nucleation sites.

Fig.1c represents topographic image of a 5x5 μm^2 area of CVD produced multilayer graphene on polycrystalline Ni substrate. Unlike polycrystalline metal, CVD grown graphene produces uneven distribution of graphene layers that covered both Ni grain and Ni interfacial grain boundaries. Nevertheless, there are some regions where graphene is relatively uniform and flat, referred to as "grains". The rest regions that lie between two or more grains regions and comprises defects and steps are referred as interface grain boundary[32] "IB". We measured average roughness of grain region for 500 x 500 nm^2 of nearly Ra = 3 nm and for IB region (500 x 500 nm^2) of Ra = 5.9 nm. Figure. 1(d) shows friction force map (nN) carried out parallel during the topography acquisition at panel (c). It is obtained by subtracting lateral force felt by AFM probe moving in trace direction from re-trace direction (i.e. trace/2- re-trace/2). This standard technique is useful to minimize the topographical influence of the sample over friction signals. It is observed that friction force (F_L) is lower at graphene IB than at grain regions (Fig. 1(d)), in contrast to friction force observed at bare Ni metal, at Ni facet, and grain boundary metal, fig 1(b). Over all figure 1 reveals that IB region may have higher accumulation of carbon layers that increases the roughness and might significantly influence the frictional characteristics of the whole composite. We will validate our observation in the following section

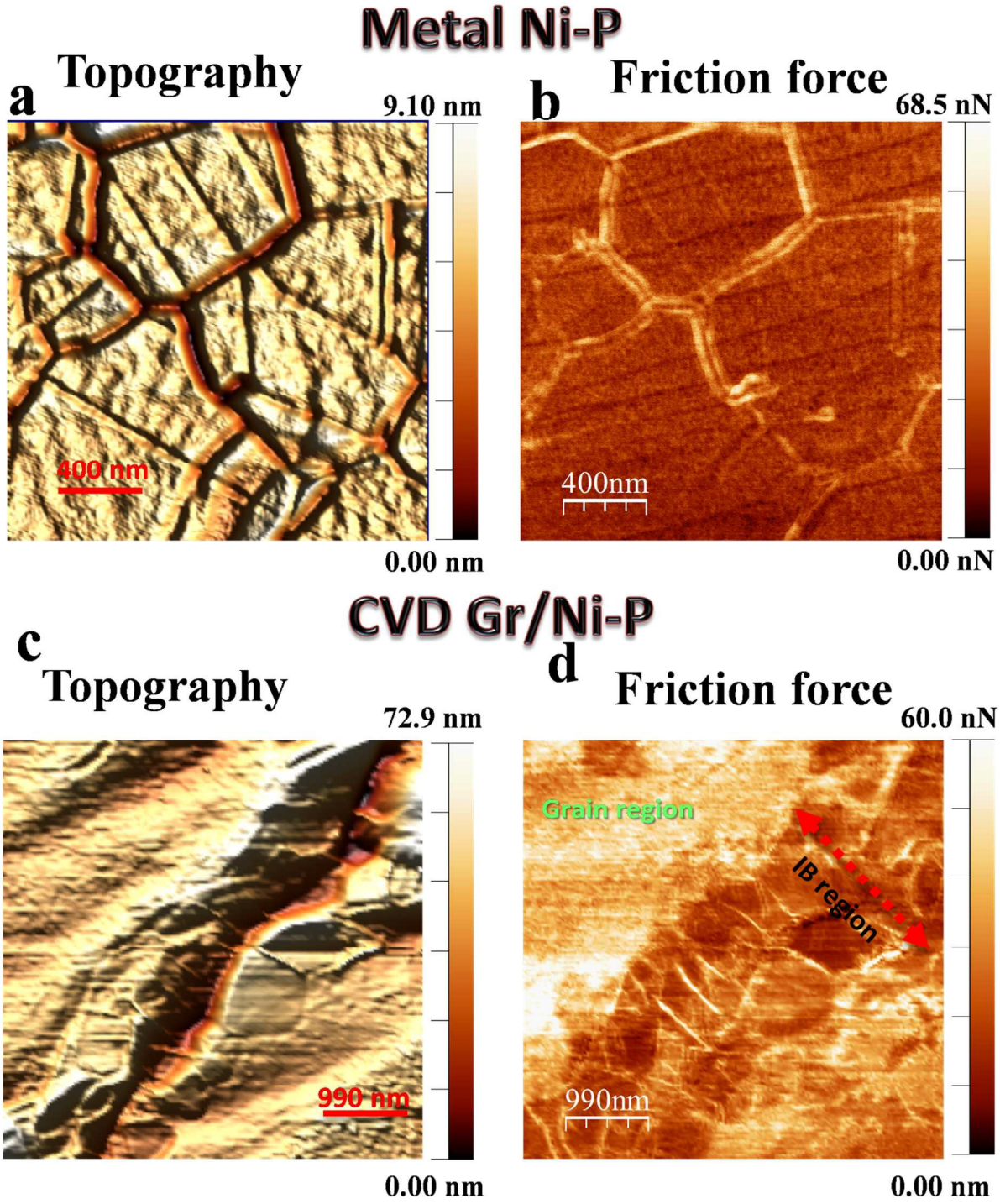

Figure 1: **Topography of polycrystalline Ni metal, bare and covered with graphene layers** (a) 3-D topography of bare Ni metal carried out with AFM (contact mode) showing Ni grain surrounded by interface boundary. (b) Friction force map measured on the same Ni region of panel (a) showing higher friction values (bright colour) at grain boundaries respect to Ni grains. (c) 3-D AFM topography image of a 5x5 μm^2 graphene region measured in contact mode. (d) Friction force map measured in parallel during the topography acquisition and obtained by the standard Trace Minus Retrace technique (TMR) analysis. Direct comparison of panel (c) and (d) reveals that the IB region, which lies along the diagonal of topography image, corresponds to low friction region of the friction map.

Figure 2 reveals comprehensive details of the same selected region of few layers Gr/Ni-P under different instrumental set-up of optical microscope (panel a), SEM (panel b), AFM topography (panel c) and friction force map (panel d). The optical contrast (Fig. 2(a)) corresponds to reflection tendency of the surface and to variable graphene thickness. The bright colour correlates to few layers graphene covered Ni grain region while the IB regions appear relatively dark. The contrast on SEM micrograph (Fig. 2(b)) of Gr/Ni-P shows the typical structure of this material composed of terraces, grain domains, IBs and step edges. The contrast image of SEM for Gr/Ni-P is the result of the amount of secondary electrons that are generated in upper few nanometers of the sample surface. Further, a high secondary electron yield is expected for Ni as compared to carbon; Ni appears brighter in the SEM image[33]. Therefore, areas that are dark in the SEM image are covered by larger number of graphene layers. The brighter contrast arises from secondary electrons that can still escape from underlying Ni substrate.

Figure 2 (c) is AFM topographical view (15 x15 μm^2) in contact mode corresponding to the marked rectangle of panel (b), its topography data by a local derivative filter present in supporting information, S1. The large bright region in panel (a) and (b) corresponds with the flat area visible in the centre of the AFM image. While, the darker regions correlates to IB regions which are relatively higher in height of graphene layers and are rougher than grain regions. Inhomogeneous distribution of the graphene

layers is dependent on orientation and size of Ni grains underneath, which produces different diffusion rate of carbon to the surface[32].

Figure 2 (d) represents friction force map measured on the same region of panel (c). The friction contrast reveal high friction zone at the centre of the image which seems to correspond with flat part of panel (c) while lower friction signals are observed at surrounding of flat grains which are IBs. The topographical description of encircled IB is mentioned in supporting information, S2. Figure 2 (e) shows overlapping of topographic and friction force mask having range from (10-30 nN) that clearly distinguishes friction force generate at grains and IBs.

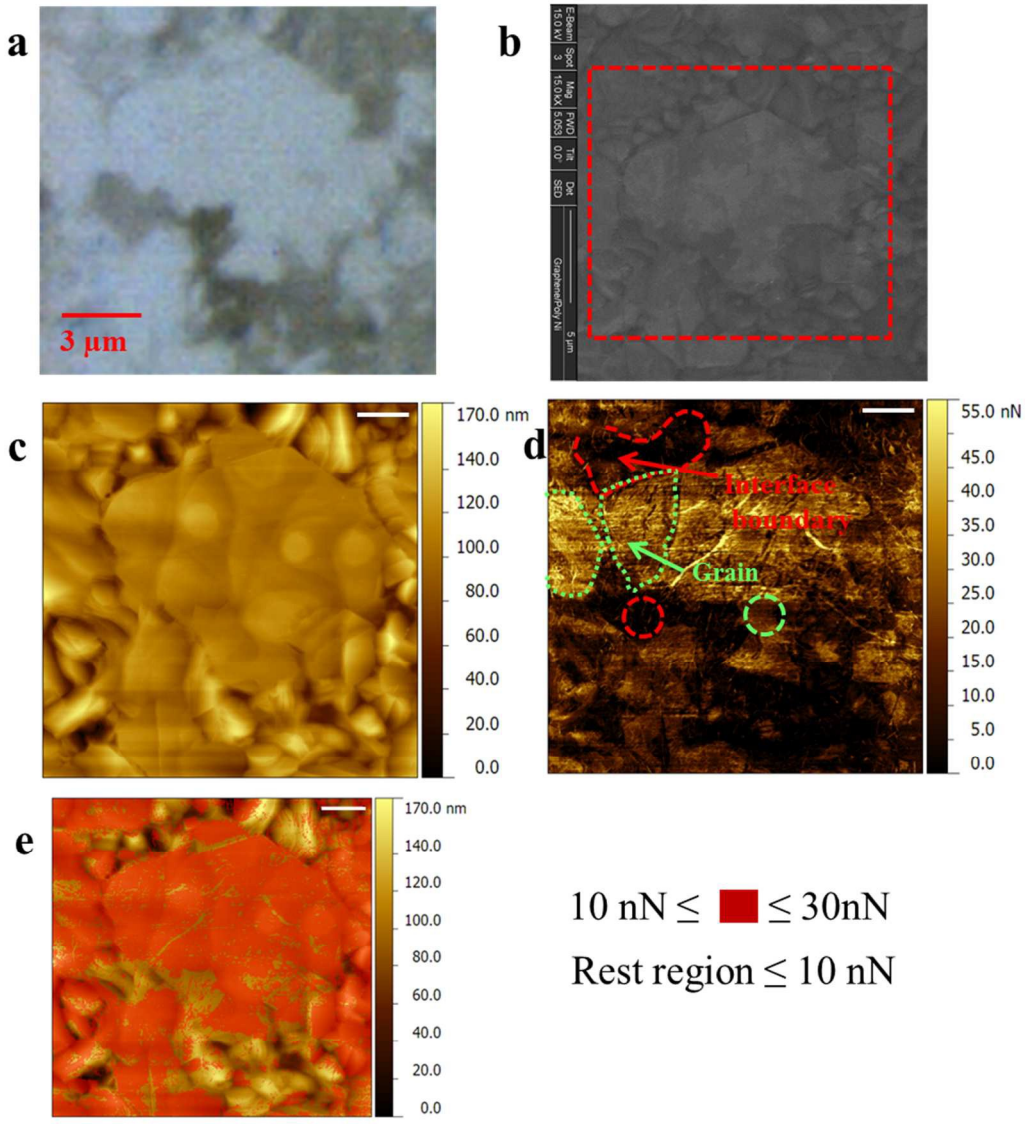

Figure 2: **Topology and friction map correlation for specific Gr/Ni-P region in optical microscope, SEM and AFM set-up** (a) Optical image (objective lens 50 X resolutions) ~ 15x15 µm^2 of Gr/Ni-P shows optical contrast due to variable graphene distribution from grain and IB. (b) SEM image (20 x 20 µm^2), contrast in SEM micrograph indicate different thickness of graphene films, details are described in text. (c) AFM topographic image (15x15 µm^2) measured in contact mode (height channel) corresponding to marked region in panel (b). (d) Friction force map measured in parallel during the topography acquisition and obtained by the TMR analysis. The encircled regions of green and red colours represent

grain and IB respectively. (e) Overlapping of topography and friction map, the red dots represent areas characterized by friction values between 10 and 30 nN.

Friction contrast under consistent F_N could also originate due to anisotropy in friction with graphene covered polycrystalline Ni. The Ni domains are randomly oriented and epitaxial grown graphene follows similar fashion[32]. F_L measurement is established as powerful tool used to differentiate between grain and Gb of metal foil like Cu[18], Ni or Gr/Ni-P. Recently, Marsden *at el*.[18] demonstrated the applicability of F_L map for better spatial resolution over SEM image where F_L contrast occurs due to difference in thickness of graphene layers. It could also originate from differences in material interaction, i.e. contrast that arise from difference in chemical interaction between the sliding tip and the surface. Hence, colour contrast ascending from F_L is not sufficient information to classify graphene thickness. The same region of figure 2 has been observed in Raman spectrometer along with reference material like1L graphene on silica and 1L graphene on Ni crystal, (supporting information, fig. S3). Raman laser was probed at two specific locations marked by dashed circles in fig. 2 (d) (area nearly 1.4 μm^2). The roughness (Ra) of these particular locations are (2.77 nm for grain) and (8 nm for IB region). Their Raman spectra are presented in supporting information, fig. S3 shows that IB are richer in carbon layers than at grain region. These collective results from roughness measurement and Raman analysis reveals that region around IB are rich in carbon layers and has significant higher roughness that may cause relatively lower contact area between sliding AFM probe and graphene. Therefore, F_L contrasts were influenced from thickness distribution and roughness of graphene layers.

Morphology influence on wettability of Gr/Ni-P. A single layer of graphene on Ni substrate shows pronounced impact on surface energy of Gr-Ni system and increases its water contact angle (WCA) towards static water droplet, which is reflected here in Fig. (3). Bare Ni substrate shows lowest WCA while graphite resulted with the highest value. Note that the presence of air born contaminants upon

exposure to ambient conditions[34] and presence of native nickel oxide leads to finite contact angle on bare Ni surface (54.4 ± 6.4°), otherwise 0° has been reported for atomically clean Ni metal[35]. The measurements for WCA carried out on various substrates representing wettability influence from different number of graphene layers, substrate effect and morphology that include roughness[36]. One layer of graphene over Ni crystal "a system that represent almost single layer graphene covered Ni free from IB" enhances the WCA to 82.4 ± 3.2° from bare Ni metal. Here, our results does not support the wetting transparency theory[37] but it does follows the phenomenon of layer independence[34,35] as it shows close resemblance with WCA between N = 1L, 4-7 L and ∞ for HOPG. Li *et al.*[34] shows weak substrate dependence for CVD produced graphene on Ni and Cu substrate using WCA values than effect from airborne impurities. Fig. 3 (b) shows variation of work of adhesion (WA) between water droplet and different samples evaluated by means of contact angle measurement and Young-Dupre equation (1). The bare Ni metal shows highest WA 115 mN/m relative to 1L Gr/Ni(111), Gr/Ni-P and graphite are ~82 mN/m, 74.7 mN/m and 73.2 mN/m respectively. These results indicate that lesser energy is required by water droplet to separate from Gr/Ni sample but lowest in case of graphite that also demonstrated elsewhere[36,38].

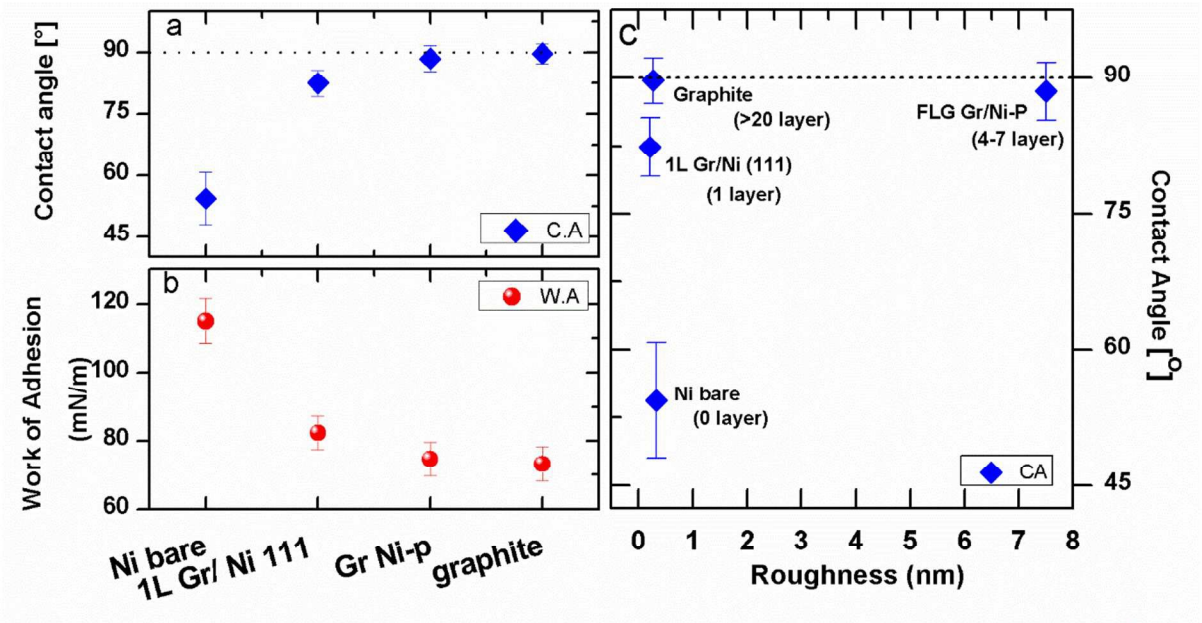

Figure 3: **Correlation between water contact angle and work of adhesion, and role of roughness of graphene layer/s** (a) Contact angle measurement using de-ionized water (~ 2 μL) over different substrates. WCA [^{o}] is decreasing with increasing number of graphene layers thus with the highest value for graphite. The error bar shows the deviation of contact angle values deviated from average dots. (b) WA between water and different substrates, the data has been taken from panel (a) and calculated through Young-Dupre equation (see text, section II). (c) WCA relates with roughness of the surface.

The relation between WCA and roughness of carbon layers shown in Fig. 3(c). It reveals that WCA values of Gr/Ni-P lies between single layer graphene and graphite. It might be possible that little enhancement in WCA has been achieved through roughness of surface aroused at IB of Gr/Ni-P. As described above single layer graphene over Ni surface raised WCA but almost preserves the roughness (Ra ≈ 0.331nm for bare Ni metal and Ra ≈ 0.22 nm for 1L Gr/Ni (111) crystal) of the substrate. Gr/Ni-P result in enhanced roughness "Ra ≈ 7.5 nm" especially at IB. 1L Gr/Ni (111) represent the system of zero% area of IB while our current sample of FLG Gr/Ni-P, IB has approximately 30.2% of area in 20x20 μm^2 size (from fig.4a). This observation is shown in Fig. (4a), where z-values (colour scale bar) from graphene covered grain is subtracted with base line correction treatment. Therefore, only amplitude (z-direction) of carbon layers at IB is shown except few humps at grain regions (amplitude < 15nm). The higher amplitude i.e. from 15nm -75 nm appears from region of IB that acts as pillars and traces are greater than 75nm. These carbon pillars have wide range of height distribution that is reflected in their roughness (Ra), fig.4 (b). Ra are the average roughness values measured from four different regions (i, ii, iii and iv) in fig.4 (a) for each of area 10 μm^2. Similar measurement was carried out at grain region that exclude pillars of IB. Ra of grains shows consistent values for Gr/Ni sample up to 20 μm^2, while it is higher and fluctuating at IB region. The surface area of graphene covered grains are measured as 800 nm^2 to 1200 nm^2. It results in an aspect ratio (i.e. height of carbon layer at IB/separation distance of IB pillars on opposite side of a grain) of about 0.022–0.066, which is not sufficient to achieve pronounced WCA

values[39]. But our current investigation evidences that using smaller metal grain size and/or enhancing height of carbon layers at IB through controlled production may result in a textured hydrophobic surface.

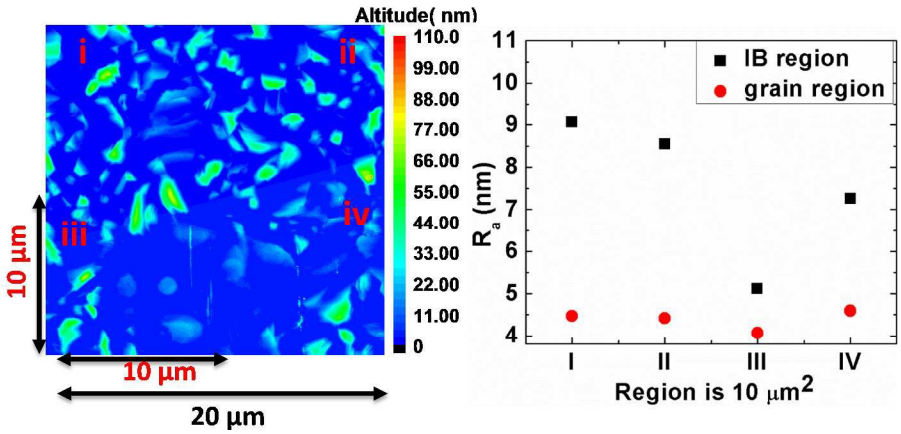

Figure 4: **Appearance of IB at Gr/Ni-P** (a) Base corrected followed by grain height subtraction AFM topography image (20x20 µm^2) of Gr/Ni-P. It shows majority of IB with relatively higher height in z-direction (>15 nm). It is divided in four different zones named as "i, ii, iii and iv" each of area 10x10 µm^2. (b) Plot of surface roughness (Ra) of four different regions (i, ii, iii and iv) of IB and grain (for grain: without base correction).

Morphological influence (Grain and interfacial grain boundary) on friction characteristics.

In order to measure friction force on a specific grain or on a IB, relatively lower scale (few nanometers) inspection is necessary. Load dependent friction measurements were carried out in vacuum (10^{-5} Torr) to avoid capillary forces[40] and the effect of air borne impurities. In this condition, friction measurement comprises only effects from sample morphology, graphene thickness and real contact condition between slider and top most graphene layer. Figure 5 shows load dependent friction measurements from single grains, on a IB and graphite (HOPG). The measurement has been conducted by ceasing the slow scan movement of cantilever while continuously scanning along the fast scan direction (about 100nm). The physical advantage of this method is that cantilever does not proceed and repeat its slide over single line

scan continuously. In this way friction data from relatively smaller IB region can be obtained. Normal force (F_N) was varied in the range from 38 nN to –22 nN by controlling the cantilever separation from the substrate. Here F_N = 0 nN stands for un-deflected cantilever, a situation where adhesion from surface gets neutralized by an applied normal deflection of the cantilever. Measurement started by applying higher deflection, then it is sequentially decreased after 60 seconds till detachment point (where tip gets separated from the surface). The overall measurement area covered was ~ 100 x 150 nm^2 due to instrumental drift along the slow scan direction and shifting of tip as function of applied displacement.

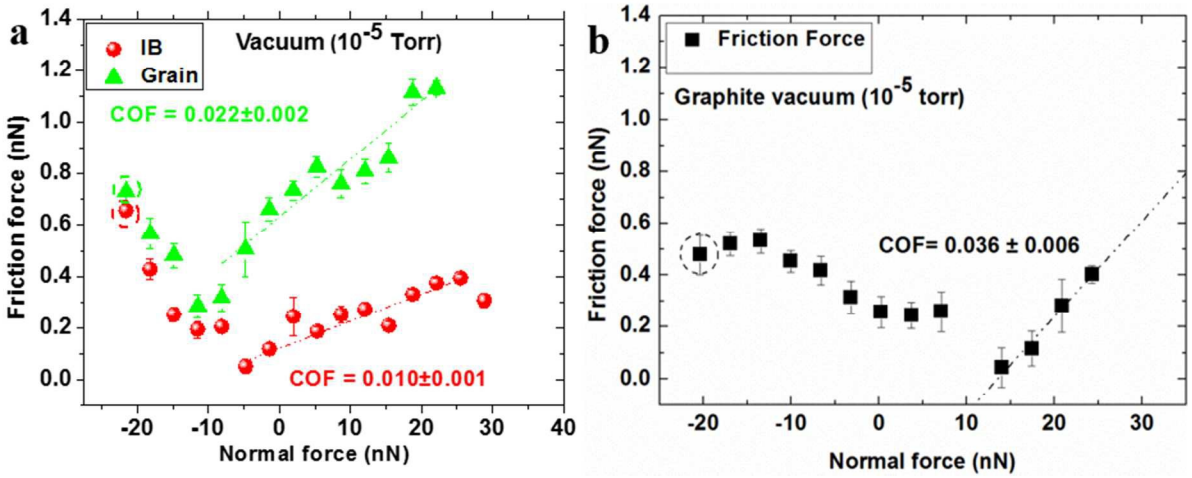

Figure 5: **Friction force at variable F_N from finite load till detachment for grain, IB and graphite**. Load dependent friction plot between silica tip and few layers graphene on (a) Gr/Ni-P (b) graphite (HOPG:- Highly Ordered Pyrolytic Graphite) carried out in vacuum (10^{-5} Torr). Panel (a) shows load dependent friction force for regions of grains and IB respectively. Linear fitt of the plot (during approach) is used to calculate COF, see text for details. The encircled values of F_N represent dynamic pull-off forces.

The lowest value of F_N when tip gets separated during lateral sliding is referred as "Dynamic pull-off force" encircled in Fig. (5). Its value in vacuum condition is nearly –22 nN for both curves of grain and IB in panel (a) and a close resemblance with graphite (≈–20.7nN) in panel (b). These values

reflect the condition of sliding tip felt similar adhesion during retraction whether from grains, IB or graphite. For all given curves presented in Fig. (5), friction force (F_F) achieves lowest values around zero F_N and increases both in either directions, whether tip is progressing towards repulsive regime or it is retracting from adhesive regime with respect to separation from the upper graphene layer. The error bar associated to each point is the standard deviation from mean value of F_F.

In the following section we discuss the evolution of F_F for progression and retraction of the sliding tip for adhesive and repulsive regime respectively. In repulsive regime, a linear fit of the curve calculated as $\left(\frac{\partial F_f}{\partial F_N}\right)$, i.e. when the tip was approaching towards surface until zero deflection (F_N = 0 nN), is defined as the COF. The COF measured in repulsive regime for IB, grain, and graphite were measured as 0.010±0.001, 0.022±0.002, and 0.036±0.006 respectively as show in fig.5 (a and b). The COF obtained from a grain region is nearly twice as much as the one obtained from IB which demonstrate lower friction characteristics of IB towards silica tip in vacuum condition. Nevertheless, the COF obtained at graphite is observed higher than those from both grain and IB. During retraction of the tip, the linear fit of the retraction part of the curve is referred as a negative COF. The negative notion apply from the fact that F_N is acting in the reverse direction than it was in the repulsive regime. The −COF obtained are from grains and IB is about equal to 0.03±0.05, which is higher than the values obtained from graphite 0.013±0.030. This particular phenomenon has been described by Deng *et al.*[23] for graphite in air condition and our results confirm this behaviour even in vacuum condition. Egbert *et al*.[19] observed similar trend of friction curve during loading and unloading of sliding tip apex for Gr-Cu system, where friction force is higher for un-loading tip than loading. It occurs when adhesion between tip apex and top most graphene layer/s is higher than exfoliation energy of sub-surface. During retraction, tip lifts the surface graphene layer/s and locally separates them from the bulk. The lifted upper layer/s are more susceptible to out-of-plane deformation than they are firmly attached to the bulk. Deformed graphene resists the sliding motion of cantilever owing to which cantilever records higher F_F[24]. In our previous work for single layer graphene on Ni (111) crystal, we did not observe this effect and unable to obtain -COF[30] which illustrate that single

layer graphene is strongly attached with Ni. The present investigation indicates that Ni metal influences the graphene layer a finite extent and might not be application for bulk (like seven layers). Nevertheless, a systematic study would be required in future to introduce graphene layers sequentially over Ni metal for measuring the extent of interfacial adhesion.

From Fig. (5), F_F at particular $F_N = -20$ nN is recorded for all curves of graphite, IB and grain are observed as 0.47 nN, 0.53 nN and 0.66 nN respectively. The choice of $F_N = -20$ nN is taken due to its importance of being a retracting force just before the detachment of cantilever. F_F value at $F_N = -20$ nN is related to the puckered size of graphene layer/s in front of sliding direction of tip apex[41]. The strength of this pucker is depends on the adhesion of the thin film to the substrate as described above. Higher F_F corresponds to greater size of puckered graphene that led to out-of-plane deformation of layer/s, which is observed higher at grain regions (F_F = 0.66 nN). Here two phenomena are dominating first, higher roughness at IB causes lower contact area at the interface unlike in graphite. There is relatively lower interaction between carbon layer and tip apex. Second, interfacial interaction between Ni metal and graphene is higher than interplanar weak vdW carbon layers in upper few layers of graphene. Therefore, for graphene covered grain, top most layers has lower interaction with its subsequent sheets that may provide higher susceptibility towards the slider. This effect has been shown by MD simulations, where inserted second graphene layer has lower interaction with 1L Gr-Ni (111) than on the slider[27]. It means that introducing more carbon layers can reduce the interfacial strength between top most sheet and Ni substrate. Note that single layer of graphene has lower bending stiffness (proportional to the cube of the thickness according to continuum mechanics) than thicker carbon layers[25]. Raman spectra (supporting information, S3, S4) showed that the number of graphene layers at grains is increased up-to 4 times. Due to finite availability of number of layers, upper thinner graphene sheet/s might be available with relatively weak interplanar forces than usual, since the bottom layers are strongly interacting with Ni substrate. This is contrast for IB and graphite where thicker graphene layers are available consequently in lesser puckered size.

FEM simulation results are summarized in Fig. (6), showing the friction force (F_F) vs. normal load (F_N) curves, and vertical deflection for graphene on grain, IB and graphite (c) at different regimes. The F_F is determined as average of the friction force recorded at the AFM tip for a displacement of 50 nm at a steady-state stabilization after the initial acceleration of the tip. During approach activity of tip, IB (red line) shows lower out-of-plane deformation that actually we can relate to higher roughness than at grain. At the withdrawing stage, simulation confirms the general trend experimentally observed of increase in the friction force: this is clearly related to higher deformability that graphene layers shows since the lower interaction, and then restrain, as they are moved away from the substrate. The lower interaction is also demonstrated by the higher area for adhesion of graphene on the tip on grains and at pull-out. The top layer of graphite deforms significantly than beneath layers, and the deformation occurs in the top 3-4 layers. The COFs obtained from linear fit of load dependent friction curves during approach of the tip are moreover in good agreement with experimental results. At withdrawing event the higher value of F_F at puckering is recorded for graphite.

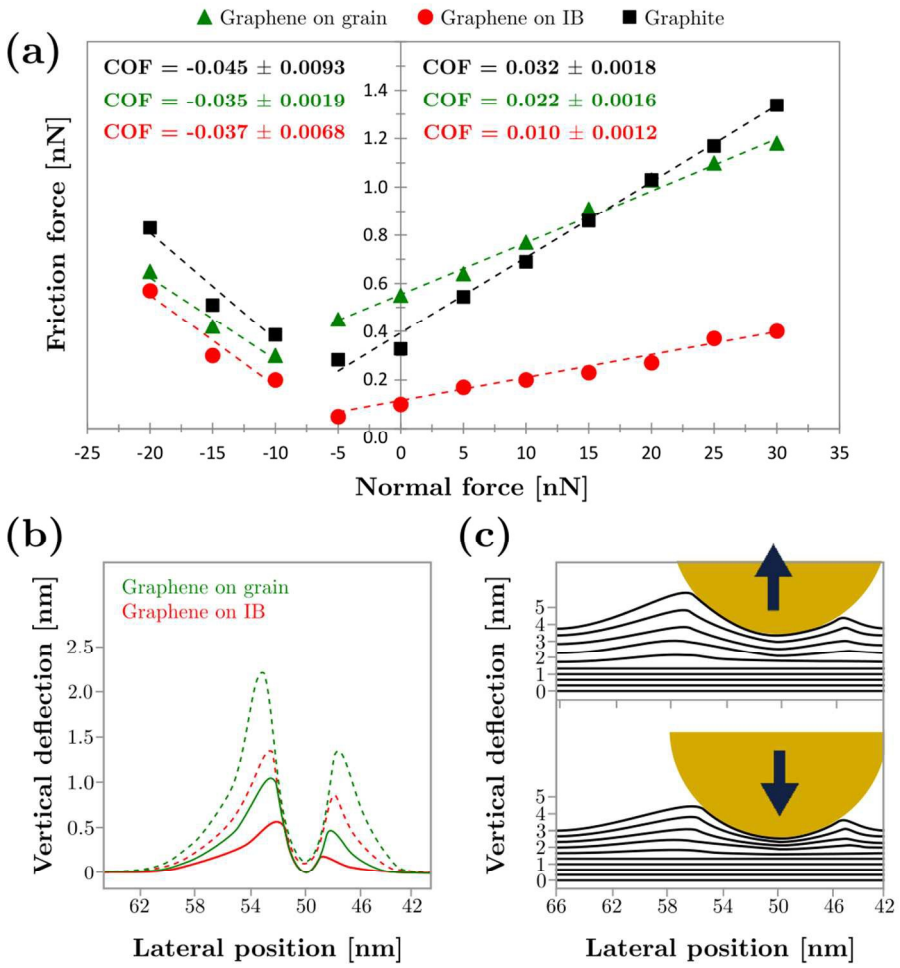

Figure 6: **Results of finite element friction simulations.** (a) F_F vs F_N results from FEM simulation on graphene covered grain, interfacial grain boundary, and graphite with estimation of the coefficient of friction for the two identified regimes. (b) Plot of the vertical deflection for single layer graphene on grain and interfacial grain boundaries corresponding to a load of +15 nN and -15 nN (negative load case corresponds to the dashed line), tip sliding towards the left-hand side, as noticeable from the asymmetric deformed shape; (c) plot of the vertical deflection of graphite in the two different regimes (-15 nN and +15 nN).

In continuation of FFM experiment, force-displacement (F-D) measurements were performed at the end of each set of friction measurements to calculate the static pull-off force. Unlike dynamic pull-off force, tip vertically approaches the surface and then retracts back, without any lateral movement. Therefore, this

part of the experiment explain the static adhesion force between tip and carbon atoms beneath it. The pull-off values obtained from F-D curve for grain and IB are −17.6 ± 0.6 nN and −15.2 ± 0.15 nN respectively. Work of adhesion, γ (i.e. work per unit area required to separate the surfaces from contact to infinity) was calculated using DMT (Derjaguin–Müller–Toporov) approximation. The interaction between AFM probe and graphene on Ni corresponds to long-range adhesion between harder materials as observed in our previous work[30] and from literature[44]. The following DMT relation between pull-off force ($F_{pull\text{-}off}$) and the work of adhesion (γ) has been considered [42]:

$$\gamma = \frac{-(F_{Pull-off})}{2\pi R} \qquad (1)$$

where R is the tip radius (≈ 8±3 nm); thus γ for grain and IB is calculated as ≈ 290 mN/m or 0.29J/m^2 and ≈ 250 mN/m or 0.25 J/m^2 respectively. Our data shows that γ decreases when roughness increases at the interface, as depicted by Jacobs and coworkers[43].

These values of static pull-off force are lower than dynamic pull-off force values obtained during sliding experiments. The discrepancy in values for "static" and "dynamic" pull-off forces is due to the fact that dynamic pull-off force occurred at deformed graphene where sliding history of tip apex plays an essential role[41]. As described, we started our measurement at higher F_N and sequentially decrease over same graphene layer at interval of 60 seconds till detachment. Therefore, before detachment of cantilever, the tip apex slides over same graphene layer between 13-15 minutes with varying load. This process locally deforms graphene at each interval and while retraction of tip can lift the graphene layer/s and locally separate them from the bulk. The lifted and puckered graphene leads to higher vertical deflection of cantilever and hence higher pull-off force[41]. While in static pull-off force, such higher deformation might not be available due to absence of sliding history and puckering might occur due to adhesion of carbon atoms.

The effect of sliding history can be avoided through reversing the direction of F_N, which can be achieved by starting F_N with lower load just before the detachment point ($F_N \approx -10$nN) and sequentially

increasing its value. Figure (7) shows load dependent friction from graphite, grain and IB. The COF of repulsive regime for IB, grain and graphite are 0.01±0.003, 0.01± 0.009 and 0.033±0.002 respectively, similar with the results presented at Fig. (5) and (6). For grain region, the slope is similar to the IB and these slope values are at the limit of the resolution of our instrument. Nevertheless, the friction force recorded is higher than obtained from IB. In adhesive regime at $F_N \approx -5$ to10nN, F_F is highest for graphite than at grain and lowest for IB, which indicate higher adhesion between graphite and the tip apex and subsequently lowering towards IB by following grain region. Graphene layer/s is not deformed significantly in the beginning and the obtained F_F values are from adhesion of contact area between tip apex and graphene carbon atoms. Obviously, higher roughness leads to lower contact area at IB resulting in lower F_F[16,44]. The magnitude of F_F shown in Figs. (5) and (7) are not comparable in adhesive regime, since in the former case friction data was affected by the sliding history as deformed graphene of unknown puckered size. While in later case, the adhesion between graphene and tip occurred with minimal deformation. Figs. (5) and (7) indicate that sliding history plays a vital role for frictional characteristic of graphene in adhesive regime during retraction of the tip. Nevertheless, the influence is insignificant for few layers graphene structure like IB and graphite in repulsive regime. Graphene friction against the silica tip showed reproducible results in repulsive regime with and without involvement of sliding history.

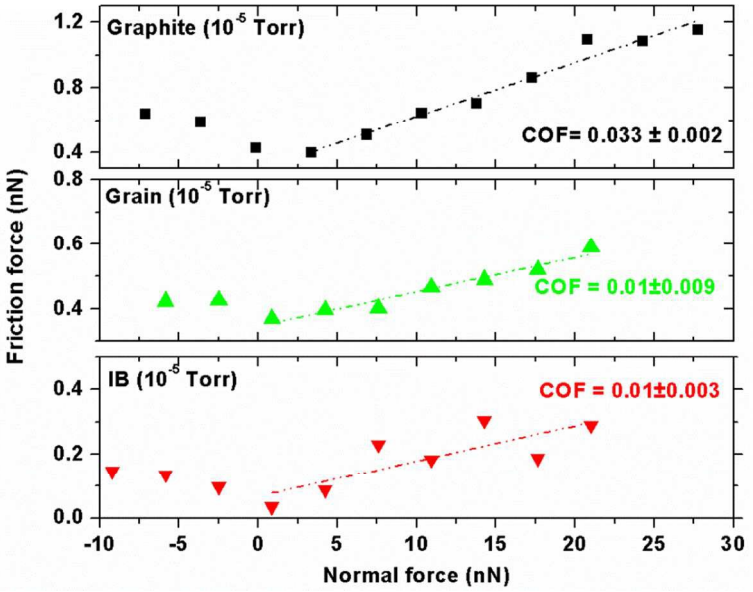

Figure 7: **Load dependent friction curve to minimize sliding history of cantilever.** Load dependent friction in vacuum (10^{-5} Torr) for graphene covered Ni IB and graphite. The applied displacement started from F_N = -10 nN and sequentially increased in order to avoid sliding history of tip over same graphene layer/s. The COF of linear part of repulsive regime for IB, grain and graphite are 0.01±0.003, 0.01±0.009 and 0.033±0.002 respectively.

The frictional characteristics of Gr/Ni-P have been compared with some reference system namely 1L graphene on Ni (111), graphite and bare Ni metal. Their respective COFs (carried out in repulsive regime) are reported in Fig. (8). These results are obtained in similar conditions to vacuum (10^{-5} Torr) with the same experimental set-up. The scatter plot was based on repeated measurements over same sample. It is clearly shown that frictional characteristics of graphene are substrate dependent whether it may be Ni (111), few layers over polycrystalline (that includes subsection of grain and IB) and graphite. The stronger interaction between native oxides of silicon tip and Ni metal (SiO_2-NiO_x) led to highest COF, which is nearly 50 times lower down with single graphene layer over Ni (111). IB has lower COF than grain and even comparable with 1L graphene on Ni (111). It means that lowest COF could be achieved through enhancement of roughness of graphene layers. Our investigation shows that integral effect from grain and IB for Gr/Ni-P causes significant drop in COF than graphite as shown by Kim *et al.*

[16] at micro scale at air condition. Our measurement at air conditions shows COF for IB and grain obtained are 0.011±0.195 and 0.018±0.018 respectively. These values are comparable with those obtained in vacuum and further validate absence of capillary effect or air borne impurities at least up to 8 hrs. Introducing higher density of IB might further decrease COF, and similar value would achieve as equivalent to 1L graphene on Ni (111). This may serve greater applied applications, since polycrystalline metal are relatively cost effective than pure crystals.

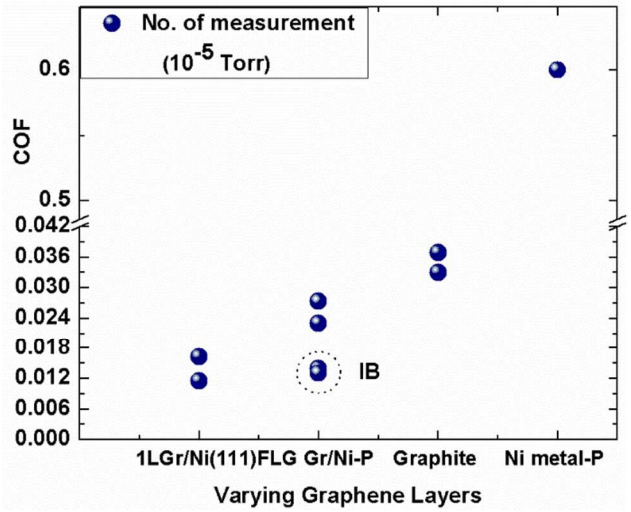

Figure 8: **Coefficient of friction for varying graphene layers distribution and morphology**. Coefficient of friction (COF) from experiments for Gr/Ni-P along with reference samples namely 1L Gr/ Ni (111), graphite and bare Ni-P metal. The COF has been obtained through linear fit of curve F_F vs. F_N recorded at the AFM tip. Each point represents a set of measurements and encircled region shows COF from IB.

Conclusion

The higher accumulation of carbon layers at IB than grains (revealed by Raman spectra) may regulate tribological characteristics of the substrate. CVD produced 1L graphene over Ni(111) resulting in significantly lower surface energy as shown in work of adhesion calculations. Gr/Ni-P offers higher WCA

due to involvement of randomly oriented few layer graphene with enhanced roughness from IB. IB roughness provides a condition of textured surface with carbon pillars/spikes, where aspect ratio is nearly 0.014–0.02 in current study. Load dependent friction carried out in vacuum (10^{-5} Torr) reveals that sliding history plays an important role to produce puckered graphene size that strongly impact on the friction force (F_F) values in the adhesive regime (when tip apex is close to detachment point). Graphene covered grain and IB is reported to lower down COF, where it is nearly half at IB than grain. COF values obtained for graphene covered grain and IB in vacuum and air conditions are similar at least up to 8 hrs of exposure to air condition. It shows Gr/Ni-P is not affected from air borne impurities and capillary effect in this duration. Roughness at IB produces favourable condition for the AFM tip to achieve lower F_F due to decrease in real contact area at the interface, that were absent in reference HOPG material used. Finite element simulation mimicking the experimental conditions, show the role of out-of-plane deformation of 1L and FLG graphene. The COF values numerically calculated are in good agreement with experimental results.

Graphene frictional characteristics depend on its out-of-plane bending stiffness. Stiffer graphene has lower susceptibility toward the slider due to high resistance for out-of-plane deformation (e.g. Gr/Ni (111)). It is established that during less interaction between the graphene and the substrate (e.g. Silica substrate), F_F is higher for single layer but relatively decreases with increasing numbers of layers due to the higher resistance to the out-of-plane deformation[21]. Our observation from FFM measurements in vacuum (10^{-5} Torr) shows that this fact might not applicable for strong interaction material with graphene. Moreover, there are other factors like roughness, interaction between graphene layers, and separation distance from Ni substrates that also plays a vital role. Introducing a limited increment of graphene layers over Ni surface (e.g. grain regions) might produce lowest interaction with top most layer since bottom layers are strongly interacting with metal (only applicable for few layers up to 4). The availability of upper layers and with lower stiffness leads to higher puckering, and consequently higher F_F. Therefore, resistance to out-of-plane deformation for graphene is the key element to minimize the F_F in FFM

measurement. The phenomenon to attain stiffer graphene should be through its subsurface not over it, as shown by functionalized graphene through fluorination[34] or hydrogenation[35], leading to higher friction force. Thus, an alternative way to minimize F_F for CVD produced graphene through its enhanced roughness contributed from interfacial grain boundary of a Ni metal was shown. Our study is applicable for all types of metal foil where graphene is partially or fully dissolved during its production.

Method

Materials. Gr/Ni-P is a multilayer graphene film supported on polycrystalline Nickel where it has been grown by chemical vapor deposition (CVD)[45]. It is a commercial sample obtained from Graphene Laboratories Inc. NY, United States (Graphene supermarket). Before starting the experiment Gr/Ni-P sample was subject to a sequential cleaning procedure with acetone and isopropyl alcohol in an ultrasonic bath for 30 minutes at 50^{o}C. Then Gr/Ni-P sample was heated in external oven at 430°C in argon flux to remove the residual impurities. The sample was inserted in AFM set-up and loaded on a temperature controlled heater stage (Enviroscope P/N: ESHTH), controlled by the Nanoscope IV unit). The AFM chamber is connected with turbomolecular pump and an oil-free scroll vacuum pump to carry out the measurement in high vacuum. Before each set of measuements Gr/Ni-P sample was heated inside AFM chamber in vacuum condition up to 250^{o}C for 2 hrs. Friction measurement was started after sample cooling down to room temperature and not more than 14 hours before heat treatment. Vacuum condition (10^{-5} Torr) was maintained from heating moment of the sample. Total number of measurements are nine carried out in vacuum condition under same instrumental set-up. All plots and COF values are reported in Fig. 5, Fig. 7 and Fig. 8. with support of FEM simulation.

Instrumentation and calibration procedure. Graphene sample has been investigated with different techniques as follows. Scanning Electron Microscope (SEM, FEI NOVA NanoSem at 5KV) and AFM-tapping mode (Enviroscope system by VEECO) were used for topographical analysis. Raman

spectroscopy (Horiba, Jobin-Yvon spectrometer model: Labram, 632.8 nm wavelength, spot diameter ~ 1μm) has been carried out to measure the graphene thickness for Gr/Ni sample. Same set-up has been used to analyze CVD produced graphene on Ni foil and transferred to Silica substrate (Gr/SiO_2-T). Friction force measurement has been carried out with same AFM apparatus operated in contact mode in vacuum condition (10^{-5} Torr). Commercially available silicon tips (MikroMasch model No.CSC37/noAl) covered with native oxide has been used for the topographic analysis as well as for friction measurement. Force-displacement (F-D) curves were systematically acquired to measure the sensitivity of photodetector that allows conversion of units from volts to nanometers using the slope of the retraction part of the curve. The comprehensive detail of this standard procedure can be found elsewhere[46]. To evaluate the force, bending and torsional spring constants of cantilever have been calculated through *Sader method* [47, 48]. Typical values are in the range of 0.3-0.4 N/m for the bending stiffness and $2\text{-}5\cdot10^{-8}$ Nm for the torsional one. Friction force (F_L) signal corresponds to the twisting of cantilever during scanning which is deduced from the lateral photodetector voltage following the procedure described in references[46, 49] with the assumption of a circular shape of laser beam on the photodetector. In that calculation, lateral sensitivity of photodetector was assumed to be equal to the sensitivity measured during normal bending of the cantilever.

The sliding of the AFM tip produces lateral force on cantilever that causes its lateral deflection in either directions (trace/retrace). The lateral signal in AFM is coupled with surface topography and induces an artefact. To minimize the topographic influence from the sample, trace and retrace scanning direction of the tip is subtracted and obtained half of "trace minus retrace" (TMR); we refer to it as "friction force" (F_L) and the mean value of F_L for a defined area as a friction force (F_F). The advantage of this approach is to minimize topological influence from the substrate during friction analysis. Experimentally, it is the width of the lateral deflection loop in trace and retrace direction of cantilever[18]. Multiple sets of measurements have been carried out through different cantilevers (similar configurations) with same calibration procedure as described above.

The static contact angle was measured using a home-made system equipped with high resolution dispenser and with CMOS camera. The measurement has been performed using 2μL of de-ionized water droplet through its image analysis[50]. Five sets of measurements have been carried out over each sample, estimating the mean values and the standard deviations. The work of adhesion of the surface was calculated using the contact angle by means of Young-Dupre's equation as follows:

$$W_A = \gamma_{lv}(1 + cos\theta) \quad (2)$$

Where, W_A is the work of adhesion, γ_{lv} is the water's total surface tension (72.8 mJ/m) and θ is the contact angle [51].

Finite element simulations. We performed 3D finite element (FEM) numerical simulations reproducing the FFM experiments in order to understand the role of the surface roughness on the adhesion of graphene sheets on Ni substrate and, consequently, in the end, on the frictional properties of the system. The planar extension of the modelled system is of 100x100 nm^2 both for graphene on Ni substrate and for graphite simulations (see supporting information Figure S5). The tip is modelled as hemispherical body with its radius equal to 8 nm, set according to the producer's specifications. The graphene layers and the substrate are fully clamped at the edges, and the Ni substrate at the bottom as well. The silica tip and the nickel substrate are modelled with solid elements. Tip, graphene sheets, and Ni substrate bodies are governed by isotropic linear elastic strain energies. Elastic properties, Young's modulus and Poisson's ratio respectively, have been assumed for silica tip E_{tip} = 170 GPa and ν_{tip} = 0.2, with density ρ_{tip} = 2.300 g/cm^3; for the nickel substrate E_{sub} = 200 GPa and ν_{sub} = 0.31 with density ρ_{sub} = 8.908 g/cm^3. The graphene sheet are modelled with fully integrated shells (2x2 Gauss point) based on Reissner-Mindlin kinematic assumption. Nominal elastic properties of graphene are assumed to be Young's modulus E_g = 1 TPa, ν_g = 0.2 and ρ_g = 1.300 g/cm^3. However, in order to not overestimate the transverse flexural stiffness of graphene in continuum models it is acknowledged that an appropriate scaling of the graphene thickness

and Young's Modulus are necessary. The FEM results match the experimental observation, using a reduced thickness of 0.066 nm, as performed also by other authors for single layer graphene[23,52] or single walled nanotubes[53,54]. Consequently, the elastic modulus must be scaled up to an effective value of 5.5 TPa.

The difference in roughness are considered in the FEM model with an equivalent sinusoidal surface of equation $z = A\sin(\lambda x)\cos(\lambda y)$ in which A and λ are assumed to have equal values to the average surface roughness R_a and $(1/4R_a)$ respectively. The interactions between the graphene layers, graphene and substrate, tip and graphene sheet have been implemented via a cohesive zone model based. The contact parameters (normal and tangential limit stress) are derived from Lennard-Jones (L-J) 6-12 potentials according to Jiang *et al.*[55] analogously to the method reported by Deng *et al*.[23] (Local static and dynamic friction coefficient between graphene layers, tip and substrate have been set to zero in the contact)

The simulation consists of two main steps: 1) the normal force F_N is applied on the tip and the flat sheets reaches their equilibrium configuration on the substrate via dynamic relaxation; 2) the sliding steps takes place with an imposed horizontal displacement on the tip. This displacement is imposed on an auxiliary node which is linked to the top of the tip hemisphere via a linear horizontal spring of rigidity $k = 10$ J/m^2. The friction force F_L is measured from the force recorded in the spring. In order to avoid boundary effect the displacement domain of the tip is limited so that the distance between its apex and the boundaries is not lower than 25 nm (50 nm of overall excursion).

Acknowledgement

NMP is supported by the European Research Council (ERC StG Ideas 2011 BIHSNAM no. 279985 on "Bio-Inspired Hierarchical Super Nanomaterials", ERC PoC 2015 SILKENE no. 693670 on "Bionic silk with graphene or other nanomaterials spun by silkworms", ERC PoC 2013 KNOTOUGH no. 632277 on "Super-tough knotted fibres"), by the European Commission under the Graphene Flagship (WP10 "Nanocomposites", no. 604391) and by the Provincia Autonoma di Trento ("Graphene nanocomposites", no. S116/2012-242637 and reg. delib. no.

2266). SS acknowledges support from BIHSNAM. GP and SV like to acknowledge Regione Emilia Romagna, Project INTERMECH – MO.RE and EU COST Action MP1303.

Supporting Information Available:

Filtered derivative of raw topographic data to distinguish between flat and rough surfaces that correspond to grain and interfacial grain boundaries respectively. AFM intermittent contact mode showing high resolution topography interfacial boundary between two grains. Raman spectra of epitaxial graphene on polycrystalline Ni that include its grain and interfacial grain boundaries. The reference samples that include as single layer graphene epitaxial grown on Ni (111) and single layer graphene mechanically exfoliated and deposited on SiO_2 substrate. Raman spectroscopy map of epitaxial grown graphene and transferred to silica substrate. Scheme of the FEM model setup.

References

1. Geim, A. K.; Novoselov, K. S., The rise of graphene. *Nature materials* **2007,** *6*, 183-191.
2. Castro Neto, A. H.; Guinea, F.; Peres, N. M. R.; Novoselov, K. S.; Geim, A. K., The electronic properties of graphene. *Reviews of Modern Physics* **2009,** *81*, 109-162.
3. Wintterlin, J.; Bocquet, M. L., Graphene on metal surfaces. *Surface Science* **2009,** *603*, 1841-1852.
4. Kim, Y.; Lee, J.; Yeom, M. S.; Shin, J. W.; Kim, H.; Cui, Y.; Kysar, J. W.; Hone, J.; Jung, Y.; Jeon, S.; Han, S. M., Strengthening effect of single-atomic-layer graphene in metal-graphene nanolayered composites. *Nature communications* **2013,** *4*, 2114.
5. Klemenz, A.; Pastewka, L.; Balakrishna, S. G.; Caron, A.; Bennewitz, R.; Moseler, M., Atomic scale mechanisms of friction reduction and wear protection by graphene. *Nano Lett.* **2014,** *14*, 7145-52.
6. Bae, S.; Kim, H.; Lee, Y.; Xu, X.; Park, J.-S.; Zheng, Y.; Balakrishnan, J.; Lei, T.; Ri Kim, H.; Song, Y. I.; Kim, Y.-J.; Kim, K. S.; Ozyilmaz, B.; Ahn, J.-H.; Hong, B. H.; Iijima, S., Roll-to-roll production of 30-inch graphene films for transparent electrodes. *Nat Nano* **2010,** *5*, 574-578.

7. Chen, C.; Rosenblatt, S.; Bolotin, K. I.; Kalb, W.; Kim, P.; Kymissis, I.; Stormer, H. L.; Heinz, T. F.; Hone, J., Performance of monolayer graphene nanomechanical resonators with electrical readout. *Nat Nano* **2009,** *4*, 861-867.

8. Geim, A. K., Graphene: status and prospects. *Science* **2009,** *324*, 1530-4.

9. Wang, S.; Zhang, Y.; Abidi, N.; Cabrales, L., Wettability and surface free energy of graphene films. *Langmuir* **2009,** *25*, 11078-81.

10. Felts, J. R.; Oyer, A. J.; Hernandez, S. C.; Whitener, K. E., Jr.; Robinson, J. T.; Walton, S. G.; Sheehan, P. E., Direct mechanochemical cleavage of functional groups from graphene. *Nature communications* **2015,** *6*, 6467.

11. Lee, G. H.; Cooper, R. C.; An, S. J.; Lee, S.; van der Zande, A.; Petrone, N.; Hammerberg, A. G.; Lee, C.; Crawford, B.; Oliver, W.; Kysar, J. W.; Hone, J., High-strength chemical-vapor-deposited graphene and grain boundaries. *Science* **2013,** *340*, 1073-6.

12. Lee, C.; Wei, X.; Kysar, J. W.; Hone, J., Measurement of the Elastic Properties and Intrinsic Strength of Monolayer Graphene. *Science* **2008,** *321*, 385-388.

13. Shin, Y. J.; Stromberg, R.; Nay, R.; Huang, H.; Wee, A. T. S.; Yang, H.; Bhatia, C. S., Frictional characteristics of exfoliated and epitaxial graphene. *Carbon* **2011,** *49*, 4070-4073.

14. Muser, M. H.; Shakhvorostov, D., Why Thick Can Be Slick. *Science* **2010,** *328*, 52-53.

15. Berman, D.; Erdemir, A.; Sumant, A. V., Graphene: a new emerging lubricant. *Materials Today* **2014,** *17*, 31-42.

16. Kim, K. S.; Lee, H. J.; Lee, C.; Lee, S. K.; Jang, H.; Ahn, J. H.; Kim, J. H., Chemical vapor deposition-grown graphene: the thinnest solid lubricant. *ACS nano* **2011,** *5*, 5107-14.

17. Filleter, T.; McChesney, J.; Bostwick, A.; Rotenberg, E.; Emtsev, K.; Seyller, T.; Horn, K.; Bennewitz, R., Friction and Dissipation in Epitaxial Graphene Films. *Physical Review Letters* **2009,** *102*, 086102.

18. Marsden, A. J.; Phillips, M.; Wilson, N. R., Friction force microscopy: a simple technique for identifying graphene on rough substrates and mapping the orientation of graphene grains on copper. *Nanotechnology* **2013,** *24*, 255704.

19. Egberts, P.; Han, G. H.; Liu, X. Z.; Johnson, A. T. C.; Carpick, R. W., Frictional Behavior of Atomically Thin Sheets: Hexagonal-Shaped Graphene Islands Grown on Copper by Chemical Vapor Deposition. *ACS nano* **2014,** *8*, 5010-5021.

20. Berman, D.; Erdemir, A.; Zinovev, A. V.; Sumant, A. V., Nanoscale friction properties of graphene and graphene oxide. *Diamond and Related Materials* **2015,** *54*, 91-96.

21. Lee, C.; Li, Q.; Kalb, W.; Liu, X. Z.; Berger, H.; Carpick, R. W.; Hone, J., Frictional characteristics of atomically thin sheets. *Science* **2010,** *328*, 76-80.

22. Filleter, T.; Bennewitz, R., Structural and frictional properties of graphene films on SiC(0001) studied by atomic force microscopy. *Physical Review B* **2010,** *81*, 155412.

23. Deng, Z.; Smolyanitsky, A.; Li, Q.; Feng, X.-Q.; Cannara, R. J., Adhesion-dependent negative friction coefficient on chemically modified graphite at the nanoscale. *Nature materials* **2012,** *11*, 1032–1037.

24. Smolyanitsky, A.; Killgore, J. P.; Tewary, V. K., Effect of elastic deformation on frictional properties of few-layer graphene. *Physical Review B* **2012,** *85*, 035412.

25. Li, Q.; Lee, C.; Carpick, R. W.; Hone, J., Substrate effect on thickness-dependent friction on graphene. *physica status solidi (b)* **2010,** *247*, 2909-2914.

26. Das, S.; Lahiri, D.; Lee, D.-Y.; Agarwal, A.; Choi, W., Measurements of the adhesion energy of graphene to metallic substrates. *Carbon* **2013,** *59*, 121-129.

27. Cahangirov, S.; Ciraci, S.; Özçelik, V. O., Superlubricity through graphene multilayers between Ni(111) surfaces. *Physical Review B* **2013,** *87*, 205428.

28. Kwon, S.; Ko, J.-H.; Jeon, K.-J.; Kim, Y.-H.; Park, J. Y., Enhanced Nanoscale Friction on Fluorinated Graphene. *Nano Letters* **2012,** *12*, 6043-6048.

29. Dong, Y.; Wu, X.; Martini, A., Atomic roughness enhanced friction on hydrogenated graphene. *Nanotechnology* **2013,** *24*, 375701.

30. Paolicelli, G.; Tripathi, M.; Corradini, V.; Candini, A.; Valeri, S., Nanoscale frictional behavior of graphene on SiO 2 and Ni(111) substrates. *Nanotechnology* **2015,** *26*, 055703.

31. Hölscher, H.; Ebeling, D.; Schwarz, U., Friction at Atomic-Scale Surface Steps: Experiment and Theory. *Physical Review Letters* **2008,** *101*, 246105.

32. Zhang, Y.; Gomez, L.; Ishikawa, F. N.; Madaria, A.; Ryu, K.; Wang, C.; Badmaev, A.; Zhou, C., Comparison of Graphene Growth on Single-Crystalline and Polycrystalline Ni by Chemical Vapor Deposition. *The Journal of Physical Chemistry Letters* **2010,** *1*, 3101-3107.

33. Warner, J. H.; Schäffel, F.; Bachmatiuk, A.; Rümmeli, M. H., *Graphene fundamentals and emergent applications*. Elsevier: Amsterdam; New York, 2013; p 229-332.

34. Li, Z.; Wang, Y.; Kozbial, A.; Shenoy, G.; Zhou, F.; McGinley, R.; Ireland, P.; Morganstein, B.; Kunkel, A.; Surwade, S. P.; Li, L.; Liu, H., Effect of airborne contaminants on the wettability of supported graphene and graphite. *Nature materials* **2013,** *12*, 925-931.

35. Raj, R.; Maroo, S. C.; Wang, E. N., Wettability of Graphene. *Nano Letters* **2013,** *13*, 1509-1515.

36. Zang, J.; Ryu, S.; Pugno, N.; Wang, Q.; Tu, Q.; Buehler, M. J.; Zhao, X., Multifunctionality and control of the crumpling and unfolding of large-area graphene. *Nature materials* **2013,** *12*, 321-325.

37. Rafiee, J.; Mi, X.; Gullapalli, H.; Thomas, A. V.; Yavari, F.; Shi, Y.; Ajayan, P. M.; Koratkar, N. A., Wetting transparency of graphene. *Nature materials* **2012,** *11*, 217-222.

38. Kim, D.; Pugno, N. M.; Buehler M. J., Ryu, S., Solving the Controversy on the Wetting Transparency of Graphene. *Scientific Reports* **2015**, 5, 15526.

39. Seemann, R.; Brinkmann, M.; Kramer, E. J.; Lange, F. F.; Lipowsky, R., Wetting morphologies at microstructured surfaces. *Proceedings of the National Academy of Sciences of the United States of America* **2005,** *102*, 1848-52.

40. Binggeli, M.; Mate, C. M., Influence of capillary condensation of water on nanotribology studied by force microscopy. *Applied Physics Letters* **1994,** *65*, 415-417.

41. Liu, X.-Z.; Li, Q.; Egberts, P.; Carpick, R. W., Nanoscale Adhesive Properties of Graphene: The Effect of Sliding History. *Advanced Materials Interfaces* **2014,** *1*, 1300053.

42. Carpick, R. W.; Ogletree D. F.; M. Salmeron, A General Equation for Fitting Contact Area and Friction vs Load Measurements. *Journal of Colloid and Interface Science*, **1999**, 211, 395–400.

43 Jacobs, T. D. B; Ryan, K. E; Keating, P. L.; Grierson, D. S.; Lefever, J. a.; Turner, K. T.; Harrison, J. a.; Carpick , R. W. The Effect of Atomic-Scale Roughness on the Adhesion of Nanoscale Asperities: A Combined Simulation and Experimental Investigation. *Tribology Letter,* **2013**, 50, 81–93.

44. Burton, Z., Bhushan, B. (2005). Hydrophobicity, adhesion, and friction properties of nanopatterned polymers and scale dependence for micro- and nanoelectromechanical systems. Nano Letters, 5(8), 1607–1613.

45. Güneş, F.; Han, G. H.; Kim, K. K.; Kim, E. S.; Chae, S. J.; Park, M. H.; Jeong, H.-K.; Lim, S. C.; Lee, Y. H., Large-area graphene based flexible trensparent conducting films. *Nano* **2009,** *04*, 83-90.

46. Carpick, R. W.; Salmeron, M., Scratching the Surface: Fundamental Investigations of Tribology with Atomic Force Microscopy. *Chemical reviews* **1997,** *97*, 1163-1194.

47. Sader, J. E.; Chon, J. W. M.; Mulvaney, P., Calibration of rectangular atomic force microscope cantilevers. *Review of Scientific Instruments* **1999,** *70*, 3967.

48. Green, C. P.; Lioe, H.; Cleveland, J. P.; Proksch, R.; Mulvaney, P.; Sader, J. E., Normal and torsional spring constants of atomic force microscope cantilevers. *Review of Scientific Instruments* **2004,** *75*, 1988.

49. Bachmann, D.; Hierold, C., Determination of pull-off forces of textured silicon surfaces by AFM force curve analysis. *Journal of Micromechanics and Microengineering* **2007,** *17*, 1326-1333.

50. Stalder, A. F.; Kulik, G.; Sage, D.; Barbieri, L.; Hoffmann, P., A snake-based approach to accurate determination of both contact points and contact angles. *Colloids and Surfaces A: Physicochemical and Engineering Aspects* **2006,** *286*, 92-103.

51. Chakradhar, R. P. S.; Dinesh Kumar, V., Water-repellent coatings prepared by modification of ZnO nanoparticles. *Spectrochimica Acta Part A: Molecular and Biomolecular Spectroscopy* **2012,** *94*, 352-356.

52. Scarpa, F.; Adhikari, S.; Gil, A.J.; Remillat, C., The bending of single layer graphene sheets: the lattice versus continuum approach. *Nanotechnology* **2010,** *21*, 125702.

53. Yakobson, B.I.; Brabec, C.J.; Bernholc, J., Nanomechanics of Carbon Tubes: Instabilities beyond Linear Response. *Physical Review Letters* **1996,** *76*, 2511-2514.

54. Pantano, A.; Parks, D.M.; Boyce, M.C., Mechanics of deformation of single and multi walled carbon nanotubes. *Journal of the Mechanics and Physics of Solids* **2004,** *52*, 789-821.

55. Jiang, L.Y.; Huang, Y.; Jiang, H.; Ravichandran, G.; Gao, H., Hwang, K.C.; Liu, B., A cohesive law for carbon nanotube/polymer interfaces based on the van der Waals force. *Journal of the Mechanics and Physics of Solids* **2006,** *54*, 2436-2452.